Chemical Science

EDGE ARTICLE

View Article Online
View Journal | View Issue

Cite this: *Chem. Sci.*, 2019, **10**, 7964

All publication charges for this article have been paid for by the Royal Society of Chemistry

$B(C_6F_5)_3$-catalyzed dehydrogenative cyclization of *N*-tosylhydrazones and anilines *via* a Lewis adduct: a combined experimental and computational investigation†

Murali Mohan Guru, ‡ Sriman De, ‡ Sayan Dutta, Debasis Koley * and Biplab Maji *

Received 22nd May 2019
Accepted 5th July 2019

DOI: 10.1039/c9sc02492a

rsc.li/chemical-science

Tris(pentafluorophenyl)borane-catalyzed dehydrogenative-cyclization of *N*-tosylhydrazones with aromatic amines has been disclosed. This metal-free catalytic protocol is compatible with a range of functional groups to provide both symmetrical and unsymmetrical 3,4,5-triaryl-1,2,4-triazoles. Mechanistic experiments and density functional theory (DFT) studies suggest an initial Lewis adduct formation of *N*-tosylhydrazone with $B(C_6F_5)_3$ followed by sequential intermolecular amination of the borane adduct with aniline, intramolecular cyclization and frustrated Lewis pair (FLP)-catalyzed dehydrogenation for the generation of substituted 1,2,4-triazoles.

Introduction

Tris(pentafluorophenyl)borane has recently emerged as a powerful Lewis acid catalyst.[1–3] The strong Lewis acidity[2,3] at the boron center allows us to establish a wide range of organic transformations *via* C–B,[4–6] C–C,[7–10] C–N,[11,12] C–O[13,14] and C–Si[15–18] bond formations. Pioneered by Stephan and Erker, $B(C_6F_5)_3$ has gained popularity in frustrated Lewis pair (FLP) chemistry which encompasses widespread applications in organic reactions.[19–22] Indeed, numerous efforts have been devoted to the activation of alkenes and alkynes by FLPs for the formation of cyclic scaffolds.[23–25] However, in many cases, the highly desirable catalytic reaction is obstructed by the initially formed stable borate adduct.[26–28] Consequently, $B(C_6F_5)_3$ catalyzed cyclization leading to important heterocyclic scaffolds is rare.[29–32]

In this context, 1,2,4-triazoles are omnipresent heterocyclic motifs in numerous biologically active compounds[33,34] and they also have widespread applications in organic light emitting diodes,[35,36] organic photovoltaic cells, electroluminescent devices,[37,38] bi-stable resistive memory devices,[39] pesticides, and medicines.[40] Given their applications, a number of strategies have been implemented for the synthesis of 1,2,4-triazoles.[41–45] However, most of these methods are limited due to the use of a super-stoichiometric amount of reagents or oxidants, low chemo-selectivity, narrow functional group tolerance, multiple reaction steps, and the production of copious waste. And catalytic metal- and oxidant-free, step-economical processes for an efficient synthesis of substituted 1,2,4-triazoles are in demand.

Lewis acid–base adducts are potential intermediates in a multitude of transformations.[46–48] Recently, Stephan and coworkers have reported that diphenyldiazomethane, obtained from the corresponding *N*-tosylhydrazone in the presence of a base, readily forms adducts with $B(C_6F_5)_3$ (Scheme 1a).[49,50] This has shifted the gear for metal-free N_2 activation closer to reality. Conversely, the direct interaction of *N*-tosylhydrazones with $B(C_6F_5)_3$ and their application in catalytic transformations have not been reported yet.

On the other hand, environmentally benign acceptorless catalytic dehydrogenation which is highly challenging even for transition-metal complexes[51,52] is rare under metal-free conditions.[53–56] Very recently, we have presented a manganese-

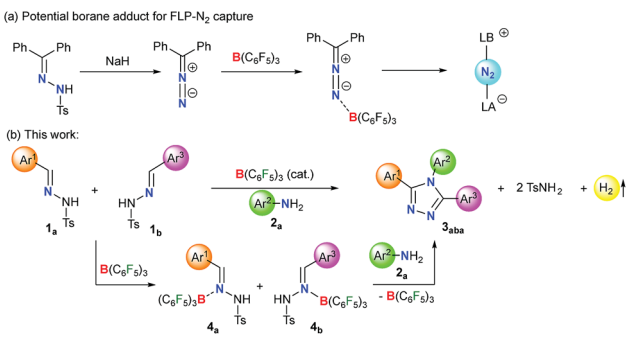

Scheme 1 Applications of borane adducts in main group chemistry.

Department of Chemical Sciences, Indian Institute of Science Education and Research Kolkata, Mohanpur-741246, India. E-mail: koley@iiserkol.ac.in; bm@iiserkol.ac.in

† Electronic supplementary information (ESI) available. CCDC 1866759. For ESI and crystallographic data in CIF or other electronic format see DOI: 10.1039/c9sc02492a

‡ These authors contributed equally to this work.

catalyzed acceptorless-dehydrogenative olefination of heteroarenes with primary alcohols.[57] Herein, we report $B(C_6F_5)_3$ catalyzed acceptorless-dehydrogenative-cyclization of *N*-tosylhydrazones **1** and anilines **2** to triaryl-1,2,4-triazoles **3** *via* a borane adduct **4** followed by sequential C–N/N–N bond formation (Scheme 1b). Furthermore, extensive DFT calculations are performed not only to understand the mechanistic features of borane catalyzed triazole formation but also to assist future development of similar classes of reactions.

Results and discussion

Initially, to check the reactivity of hydrazone $\mathbf{1_a}$ with $B(C_6F_5)_3$, a stoichiometric reaction in benzene at room temperature was carried out. It leads to the formation of a Lewis adduct $\mathbf{4_a}$ ($\delta^{11}B$ – 2.5 ppm) after 1 h in 82% yield (Scheme 2). When $\mathbf{4_a}$ was reacted with an aromatic amine $\mathbf{2_a}$ at 80 °C in benzene, 3,4,5-triaryl-1,2,4-triazole $\mathbf{3_{aaa}}$ was formed in 85% NMR yield after 12 h along with an equimolar amount of $TsNH_2$ and $B(C_6F_5)_3$.

As $B(C_6F_5)_3$ was finally released from the adduct $\mathbf{4_a}$ after its reaction with the amine $\mathbf{2_a}$, it was posited that catalytic turnover should be possible under thermal conditions. Interestingly, when the reaction was implemented with 5 mol% $B(C_6F_5)_3$ at 80 °C 1,2,4-triazole $\mathbf{3_{aaa}}$ was obtained in 82% isolated yield along with 68% of $TsNH_2$ as a byproduct (Table 1, entry 1). While the increased catalyst loading did not significantly improve the yield (entry 2), a slight decrease in the product yield was observed with 3 mol% $B(C_6F_5)_3$ (entry 3). The use of less Lewis acidic boranes such as BPh_3 was unproductive (entry 4). In addition, less hindered boranes like $BF_3{\cdot}OEt_2$ resulted in no detectable product formation (entry 5). Other Lewis acid catalysts like $Sc(OTf)_3$, $FeCl_3$ and $ZnCl_2$ were also not effective for this reaction (entry 6, Schemes S9 and S10 in the ESI†).

Next, the scope of this metal-free protocol was explored. A series of hydrazones **1** could be employed with various anilines **2** to afford symmetrical 3,4,5-triaryl-1,2,4-triazoles **3** in good to excellent yields (Table 2). The reaction of $\mathbf{1_a}$ and $\mathbf{1_b}$ with anilines $\mathbf{2_{a–f}}$ bearing OMe-, Me-, H-, Cl- and Br-substituents at the *para*- or *meta*-position of the aryl ring afforded the triazoles **3aab–3bbf** in 66–87% yields. Similarly, the hydrazones $\mathbf{1_{c–g}}$ having substituents with different steric and electronic properties at the *ortho*-, *meta*-, and *para*-position on the aromatic rings could readily be cyclized with $\mathbf{2_a}$ to produce **3cca–3gga** in 71–86% yields. Electronically biased aryl rings could be installed smoothly to obtain $\mathbf{3_{ccb}}$, $\mathbf{3_{hhb}}$, and $\mathbf{3_{iic}}$ in 56–78% yields. Likewise, thiophene- and fluorine-containing 1,2,4-triazoles $\mathbf{3_{eeh}}$ and $\mathbf{3_{jjg}}$ could be synthesized in 79% and 84% yields,

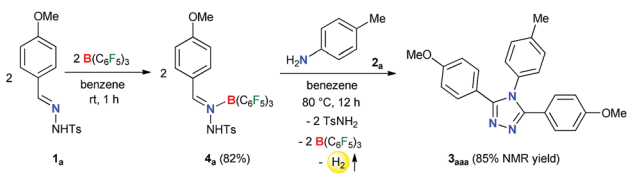

Scheme 2 Borane adduct of *N*-tosylhydrazone $\mathbf{1_a}$ and its transformation.

Table 1 Optimization of $B(C_6F_5)_3$ catalyzed cyclization of the hydrazone $\mathbf{1_a}$ with anilines $\mathbf{2_a}$[a]

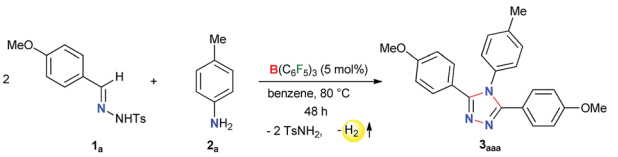

Entry	Deviation from above	Yield (%)
1	None	82 (85)[b]
2	10 mol% $B(C_6F_5)_3$	83
3	3 mol% $B(C_6F_5)_3$	74
4	5 mol% $B(C_6H_5)_3$	n.r.
5	5 mol% BF_3 OEt_2	n.r.
6	5 mol% $Sc(OTf)_3$ or $FeCl_3$ or $ZnCl_2$	n.r.

[a] Reaction conditions: $\mathbf{1_a}$ (0.5 mmol), $\mathbf{2_a}$ (0.25 mmol), and $B(C_6F_5)_3$ (5 mol%) in 2.0 mL benzene; isolated yield. [b] NMR yield using 1,3,5-trimethoxybenzene as the internal standard. n.r. = no reaction.

Table 2 $B(C_6F_5)_3$ catalyzed synthesis of symmetrical 1,2,4-triazoles[a]

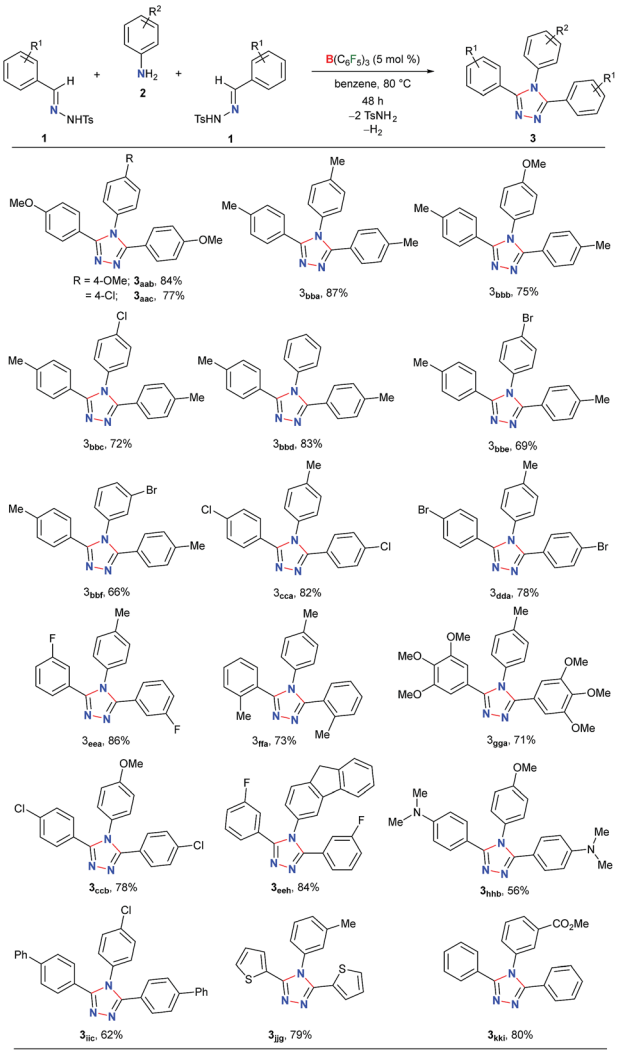

[a] Reaction conditions: Table 1, entry 1. Yields of the analytically pure product.

respectively. Notably, an ester-group could also be tolerated under the reaction conditions to furnish $\mathbf{3_{kki}}$ in 80% yield. On the other hand, substrates containing amides, nitro groups, olefins, primary alcohols, primary amino groups, *N*-tosylhydrazone of aliphatic aldehydes, and *N*-methanesulfonyl hydrazone were found to be unsuitable as either the starting materials remained intact or a complex mixture of products was formed (Schemes S1–S5 in the ESI†).

To further demonstrate the applicability of our protocol, we examined the possibility of obtaining unsymmetrical 1,2,4-triazoles by employing two different hydrazones (Table 3). In fact, the synthesis of unsymmetrically substituted 1,2,4-triazoles is considered to be highly challenging and to the best of our knowledge, their single step synthesis from readily accessible starting materials is less explored.[41–45] Gratifyingly, when $\mathbf{2_a}$ was reacted with an equimolar mixture of $\mathbf{1_a}$ and $\mathbf{1_c}$ the unsymmetrical 1,2,4-triazole $\mathbf{3_{aca}}$ was obtained as a major product in 77% yield and symmetrical triazoles were only obtained in minor amounts. The products could be purified *via* column chromatography on silica-gel using an ethyl acetate/hexane mixture as the eluent. Similar reactivity and selectivity were also observed for the synthesis of $\mathbf{3_{ada}}$ and $\mathbf{3_{aea}}$. Likewise, biphenyl-, haloaromatic- and heteroaromatic-rings could be installed without any difficulty to give the triazoles $\mathbf{3_{aic}}$, $\mathbf{3_{aja}}$, $\mathbf{3_{akc}}$, $\mathbf{3_{bcb}}$ and $\mathbf{3_{bdb}}$ in 61–80% yields. Colorless crystals of $\mathbf{3_{aic}}$, grown from a saturated benzene solution stored at room temperature, were suitable for single-crystal X-ray analysis and clearly confirmed the structure of the product (Fig. S3 in the ESI†).[58] It is noteworthy that the reaction is highly chemoselective as the reactive carbomethoxy- and cyano-groups remain unaffected under the present reaction conditions to provide $\mathbf{3_{aki}}$ and $\mathbf{3_{alb}}$ in 74% and 58% yields, respectively. The steric hindrance was found to exert a negligible influence on the reaction to give the desired product $\mathbf{3_{bga}}$ and $\mathbf{3_{bmf}}$ in good yields.

In order to obtain insight into the reaction mechanism, several equilibrium studies were performed initially with *N*-tosylhydrazones and anilines in the presence of Lewis acids (Scheme 3). At the onset, the relative Lewis basicity of aniline and *N*-tosylhydrazone towards $B(C_6F_5)_3$ was analyzed (Scheme 3a). Thus, in a stoichiometric reaction of $\mathbf{2_a}$ and $B(C_6F_5)_3$ at room temperature in C_6D_6, the ratio of $\mathbf{2_a}$ and $\mathbf{5_a}$ ($B(C_6F_5)_3$ adduct of $\mathbf{2_a}$) was found to be 1 : 4 ($\mathbf{2_a} : \mathbf{5_a} = 1 : 4$). Similarly, the stoichiometric mixture of $\mathbf{1_a}$ and $B(C_6F_5)_3$ in C_6D_6 at room temperature afforded quantitative formation of $\mathbf{4_a}$ ($B(C_6F_5)_3$ adduct $\mathbf{1_a}$) where the ration was $\mathbf{1_a} : \mathbf{4_a} = 0 : 100$. This confirms the tendency of *N*-tosylhydrazone **1** to form a stronger Lewis acid–base adduct with $B(C_6F_5)_3$ in comparison to aniline **2**.

Table 3 $B(C_6F_5)_3$ catalyzed synthesis of unsymmetrical 1,2,4-triazoles[a]

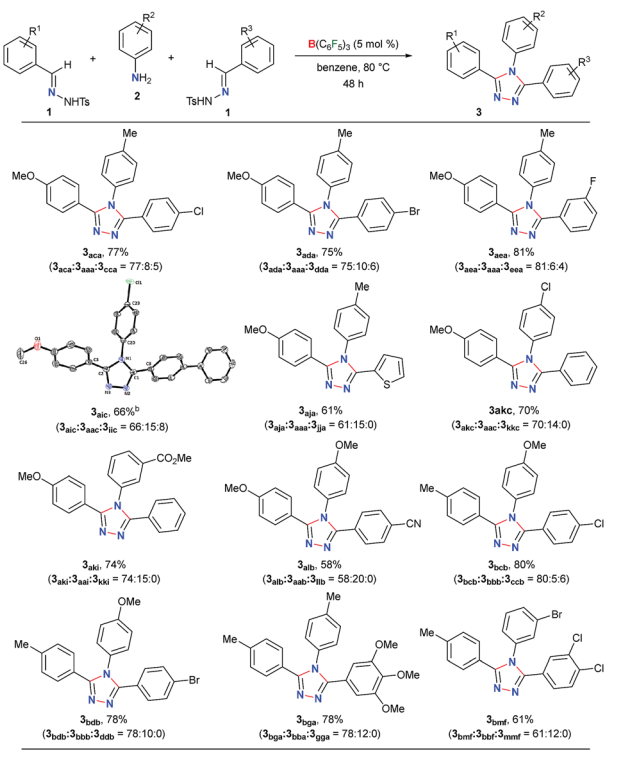

[a] Reaction conditions: Table 1, entry 1 in the 0.5 mmol scale. Yields of the analytically pure product. Selectivities are given within parenthesis. [b] Thermal ellipsoids are shown at a 60% probability level. Ref. 58.

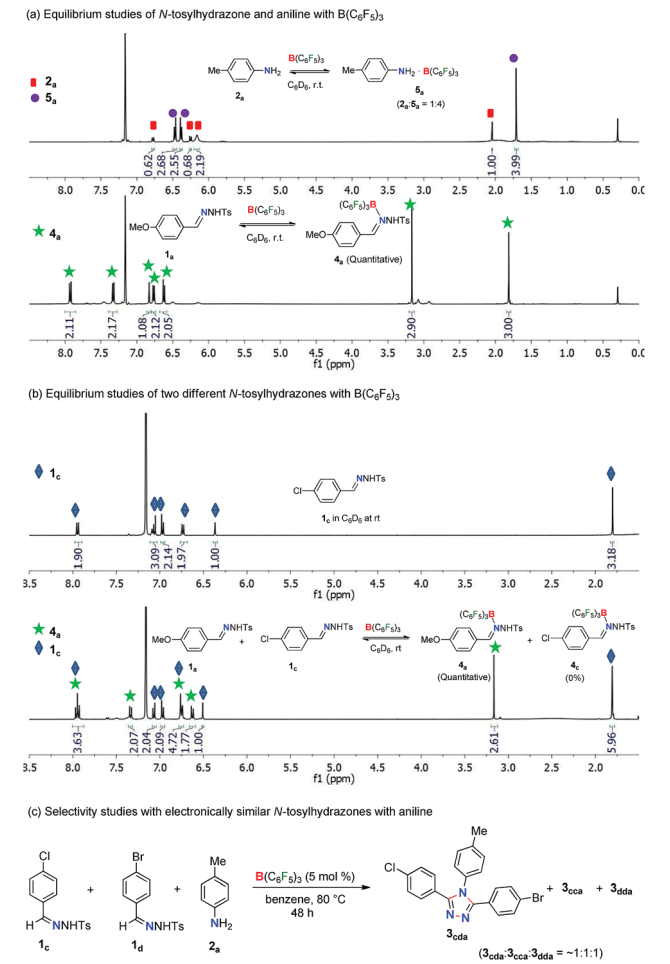

Scheme 3 Equilibrium and selectivity studies for 1,2,4-triazole formation.

Moreover, a competitive equilibrium study was performed with two electronically biased *N*-tosylhydrazones ($\mathbf{1_a}$ *vs.* $\mathbf{1_c}$) with $B(C_6F_5)_3$ (Scheme 3b). Accordingly, a stoichiometric (1 : 1) mixture of $\mathbf{1_a}$ and $\mathbf{1_c}$ was treated with 1 equivalent of $B(C_6F_5)_3$ in C_6D_6 at room temperature. This selectively afforded the Lewis acid–base adduct $\mathbf{4_a}$ whereas $\mathbf{1_c}$ remained unreacted ($\mathbf{4_a} : \mathbf{1_c}$ = 1 : 1). Thus, *N*-tosylhydrazones having electron rich arenes will form strong Lewis acid–base adducts than hydrazones having electron deficient arenes. This is possibly a crucial factor for the selectivity observed during the synthesis of unsymmetrical 1,2,4-triazoles as shown in Table 3. Along this direction, in fact, the reaction of aniline $\mathbf{2_a}$ with a mixture of $\mathbf{1_c}$ and $\mathbf{1_d}$ having electronically similar substituents (Cl and Br) on arenes in the presence of the $B(C_6F_5)_3$ catalyst provided a mixture of two symmetrical and unsymmetrical 1,2,4-triazoles (Scheme 3c) as both the hydrazones have similar probabilities for the formation of Lewis acid–base adducts with $B(C_6F_5)_3$. Thus, electronically biased hydrazones are good candidates for better selectivity of unsymmetrical triazoles.

In the case of competitive equilibrium studies of two different anilines with $B(C_6F_5)_3$, a stoichiometric (1 : 1 : 1) mixture of $\mathbf{2_a}$, $\mathbf{2_c}$ and $B(C_6F_5)_3$ in C_6D_6 at room temperature gave their corresponding Lewis acid–base adduct $\mathbf{5_a}$ and $\mathbf{5_c}$, respectively in an 8 : 1 ratio (Scheme S8 in the ESI†). This indicates that highly basic anilines will form stronger adducts with $B(C_6F_5)_3$. It is also noteworthy that other Lewis acids like $Sc(OTf)_3$ and BPh_3 did not form any Lewis acid–base adducts with *N*-tosylhydrazones or anilines under similar reaction conditions (Schemes S9 and S10 in the ESI†).

In addition, the kinetic isotope effect (KIE) of 1.0 measured from a parallel reaction of $\mathbf{2_a}$ with $\mathbf{1_a}$ and its deuterated analogue **1a-[D]** suggests that the breakage of the imine C–H bond of $\mathbf{1_a}$ is not involved in the rate-determining step (Scheme 4a). Kinetic monitoring of the reaction suggests an exponential decay of both the reactants $\mathbf{1_a}$ and $\mathbf{2_a}$, whereas sigmoidal increase of $\mathbf{3_{aaa}}$ was observed (Fig. S1 in the ESI†). The initial rate curve for triazole product formation possibly indicates that at the beginning, product formation is slower due to accumulation of reactive intermediates. Further kinetic studies revealed that the reaction is first order in the catalyst (Scheme S11 in the ESI†) and aniline $\mathbf{2_a}$ (Scheme S12 in the ESI†), and zero order in the *N*-tosylhydrazone $\mathbf{1_a}$ (Scheme S13 in the ESI†). In addition, the electronic influence of the aryl-substituents on both the reactants was investigated by a Hammett correlation study (Scheme 4b). By varying different electronic groups on the aryl-ring of **2** a small $\rho = -1.17$ was obtained. This plausibly indicates a weak resonance interaction involving a positive-charge at the N center of aniline in the rate-determining-step. On the other hand, a negligible substituent effect ($\rho = -0.16$) was determined for *N*-tosylhydrazones. Meanwhile, the evolution of H_2 gas as a byproduct was confirmed by the transfer hydrogenation[59,60] of styrene under the reaction conditions (Scheme 4c). A 2 : 1 : 1 mixture of $\mathbf{1_a}$, $\mathbf{2_a}$ and styrene in the presence of the $B(C_6F_5)_3$ catalyst afforded 82% of $\mathbf{3_{aaa}}$ along with 68% of ethylbenzene (Scheme 4c). Moreover, we performed a number of control experiments using amidines, azines, and imines as possible reaction intermediates albeit none of them proceeded to give 1,2,4-triazoles (Schemes S14–S16 in the ESI†).

A plausible mechanism is proposed on the basis of the above experimental observations and previous literature reports (Scheme 5).[54,55] To the best of our knowledge DFT calculations of N–N cyclization leading to 1,2,4 triazole fragments are obscure. Based on the proposed mechanism of the $B(C_6F_5)_3$-catalyzed acceptorless-dehydrogenative-cyclization of *N*-tosylhydrazones with anilines (Scheme 5), we have performed DFT calculations to investigate the detailed reaction mechanism and to gain insight into the driving force for the formation of the 1,2,4-triazole moiety $\mathbf{3_{bba}}$. Additionally, the calculations seek to address some pertinent questions regarding the studied system: (a) the specific role of $B(C_6F_5)_3$ in the reaction, (b) the rate-limiting-step in the reaction, and (c) product distribution for unsymmetrical coupling.

The reaction is initiated with the coordination of $B(C_6F_5)_3$ to the sp^2 nitrogen (N^1) in *N*-tosylhydrazone ($\mathbf{1_b}$) which results in

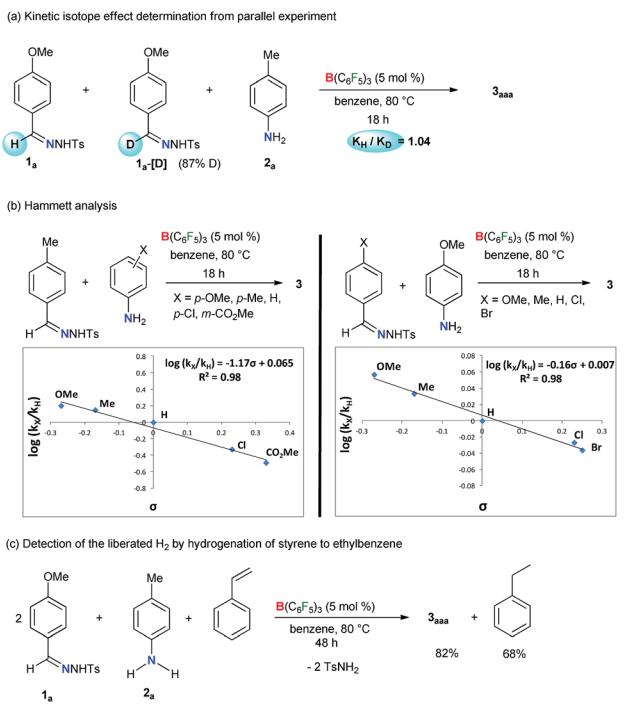

Scheme 4 Kinetic and mechanistic studies for the synthesis of 1,2,4-triazole.

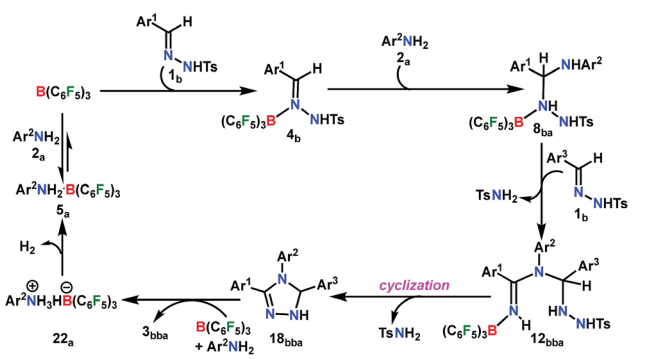

Scheme 5 Plausible reaction mechanism.

the formation of an isoenergetic encounter complex $\mathbf{4_b^P}$ (Scheme 6). The approach of the nucleophilic N^1 center in $\mathbf{1_b}$ towards the electron-deficient B center in $B(C_6F_5)_3$ furnishes the slightly more stable Lewis adduct $\mathbf{4_b}$ *via* a transition state $\mathbf{[4^P\text{-}4]_b^{\ddagger}}$ with an activation barrier of 10.9 kcal mol^{-1}. Despite the fact that the N^2 center in $\mathbf{1_b}$ is significantly electron-rich (−0.646 e) compared to the N^1 center (−0.242 e), as obtained by the natural population analysis (NPA), $B(C_6F_5)_3$ gets coordinated to the N^1 center. This is attributed to the fact that the lone pair orbital located on the N^1 atom (HOMO-4) is significantly destabilized compared to the one on the N^2 atom (HOMO-5) by 0.4 eV (Fig. S100 in the ESI†). Furthermore, coordination at the N^2 center resulted in adduct **4b′**, which is less stable than $\mathbf{4_b^P}$ by 2.4 kcal mol^{-1} (Scheme S17 in the ESI†).

To cast light on the origin of the activation barrier and the bonding scenario in $\mathbf{[4^P\text{-}4]_b^{\ddagger}}$, EDA-NOCV (energy decomposition analysis-natural orbital for chemical valence) analysis was performed, considering $\mathbf{1_b}$ and $B(C_6F_5)_3$ as interacting fragments (Table S4 in the ESI†). Examination of the individual energy terms of the EDA reveals that the B–N^1 bond has a higher electrostatic character (ΔE_{elstat}: 39.8%) than the covalent character (ΔE_{orb}: 33.5%). Importantly, the major contribution to the total covalent interaction (ΔE_{orb}) originates from the donation of the lone pair on the N^1 center in $\mathbf{1_b}$ to the vacant $2p_z$ orbital of boron in the $B(C_6F_5)_3$ fragment (Fig. S101 in the ESI†). We have calculated the associated eigenvalue of 0.49 e quantifying the amount of charge flow from donor → acceptor fragments. Additionally, the $B(C_6F_5)_3$ fragment has the predominant contribution to the destabilizing distortion energy (ΔE_{dis}). The calculated electron density [ρ(r)] of 0.112 at the (3, −1) bond critical point (BCP) of the B–N^1 bond in $\mathbf{4_b}$ along with the respective Laplacian of +0.192 [$\nabla^2\rho$(r)] suggests a donor–acceptor type interaction.[61,62] Thereafter, the coordination of the substituted aniline ($\mathbf{2_a}$) to $\mathbf{4_b}$ affords the intermediate $\mathbf{6_{ba}}$ which finally leads to a slightly more stable Zwitterionic complex $\mathbf{7_{ba}}$ accompanied by a moderately low energy barrier of 8.8 kcal mol^{-1}. The imaginary mode in $\mathbf{[6\text{-}7]_{ba}^{\ddagger}}$ portrays the formation of the C–N^3 bond (1.849 Å) along with concomitant elongation of the C–N^1 bond (1.383 Å). It is worthwhile to mention that the HOMO in $\mathbf{7_{ba}}$ represents the lone pair orbital located on the N^1 atom (Fig. S100 in the ESI†). The subsequent proton transfer from N^3 to the N^1 center in $\mathbf{7_{ba}}$ furnishes the significantly less stable intermediate $\mathbf{8_{ba}}$ *via* a four-membered transition state $\mathbf{[7\text{-}8]_{ba}^{\ddagger}}$ (Scheme 6, Fig. 1a). The step $\mathbf{7_{ba}} \rightarrow \mathbf{8_{ba}}$ involving proton migration requires an activation barrier of 32.0 kcal mol^{-1} and thus becomes the rate-limiting step for the overall transformation.[63] Indeed, this is supported by the experimental rate curve with a slower rate at the beginning of the reaction (*vide supra*, Fig. S1 in the ESI†). The single imaginary mode in $\mathbf{[7\text{-}8]_{ba}^{\ddagger}}$ depicts the synchronous breakage of N^3–H (1.296 Å) and formation of N^1–H (1.353 Å) bonds. In $\mathbf{[7\text{-}8]_{ba}^{\ddagger}}$, the B–$N^1$ bond gets significantly elongated (1.602/1.676 Å in $\mathbf{7_{ba}}$/$\mathbf{[7\text{-}8]_{ba}^{\ddagger}}$) and this weakening of the donor–acceptor bond is reflected in the reduced NPA charge on the B center (+0.467/+0.488 e in $\mathbf{7_{ba}}$/$\mathbf{[7\text{-}8]_{ba}^{\ddagger}}$). It should be noted that both aniline and $TsNH_2$ assisted alternative intermolecular proton transfer between the two nitrogen centers ($N^3 \rightarrow N^1$) are less favorable than the intramolecular path reported in Scheme 6 (Scheme S18a and b in the ESI†).

From here on, the coupling of a second *N*-tosylhydrazone unit is required for the progress of the reaction. This is accomplished through an initial proton transfer from the C center in $\mathbf{8_{ba}}$ to N^4 in $\mathbf{1_b}$. Such a proton abstraction from the tertiary C atom is manifested with N^1–N^2 bond elongation. This intermolecular proton transfer is clearly favorable (−17.5 kcal mol^{-1}), creating charged species $\mathbf{1_b^+}$ and $\mathbf{9_{ba}}$ respectively (Scheme 7), whereas the coordination of $\mathbf{1_b}$ instead of proton transfer is highly unfavorable (refer Scheme S18c in the ESI†). In accordance with the experimental findings, KIE measurements suggest the non-involvement of imine C–H bond cleavage in the rate-determining step (Scheme 4a). Though obvious, it is important to note that hydrogen abstraction from electronegative N centers in $\mathbf{8_{ba}}$ is undoubtedly difficult, leading to highly unstable intermediates (Scheme S18d in the ESI†). Close inspection of the structural parameters in $\mathbf{9_{ba}}$ indicates considerable elongation, rather than

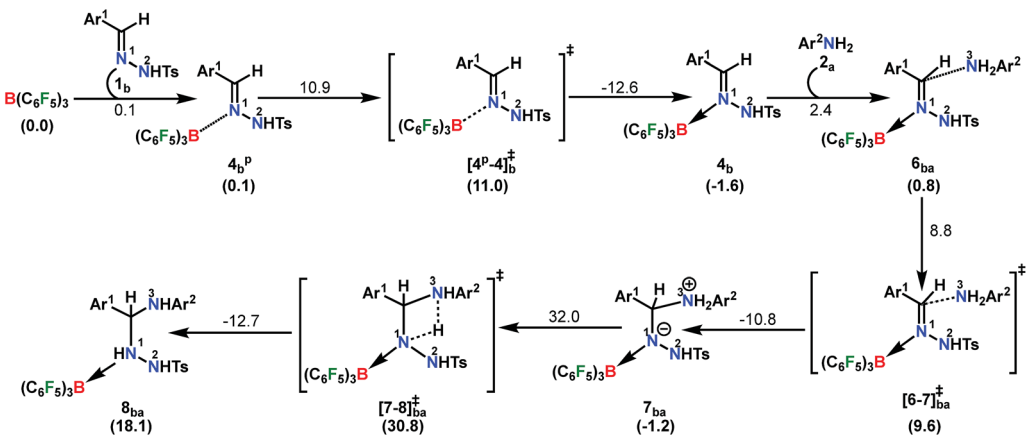

Scheme 6 Part I: the reaction pathway for the formation of the intermediate $\mathbf{8_{ba}}$. The energy values above the arrows denote the Gibbs free energy changes (ΔG_L^S) of the individual steps. The values within parentheses are the relative ΔG_L^S energies w.r.t the starting structures. All energy terms are in kcal mol^{-1}.

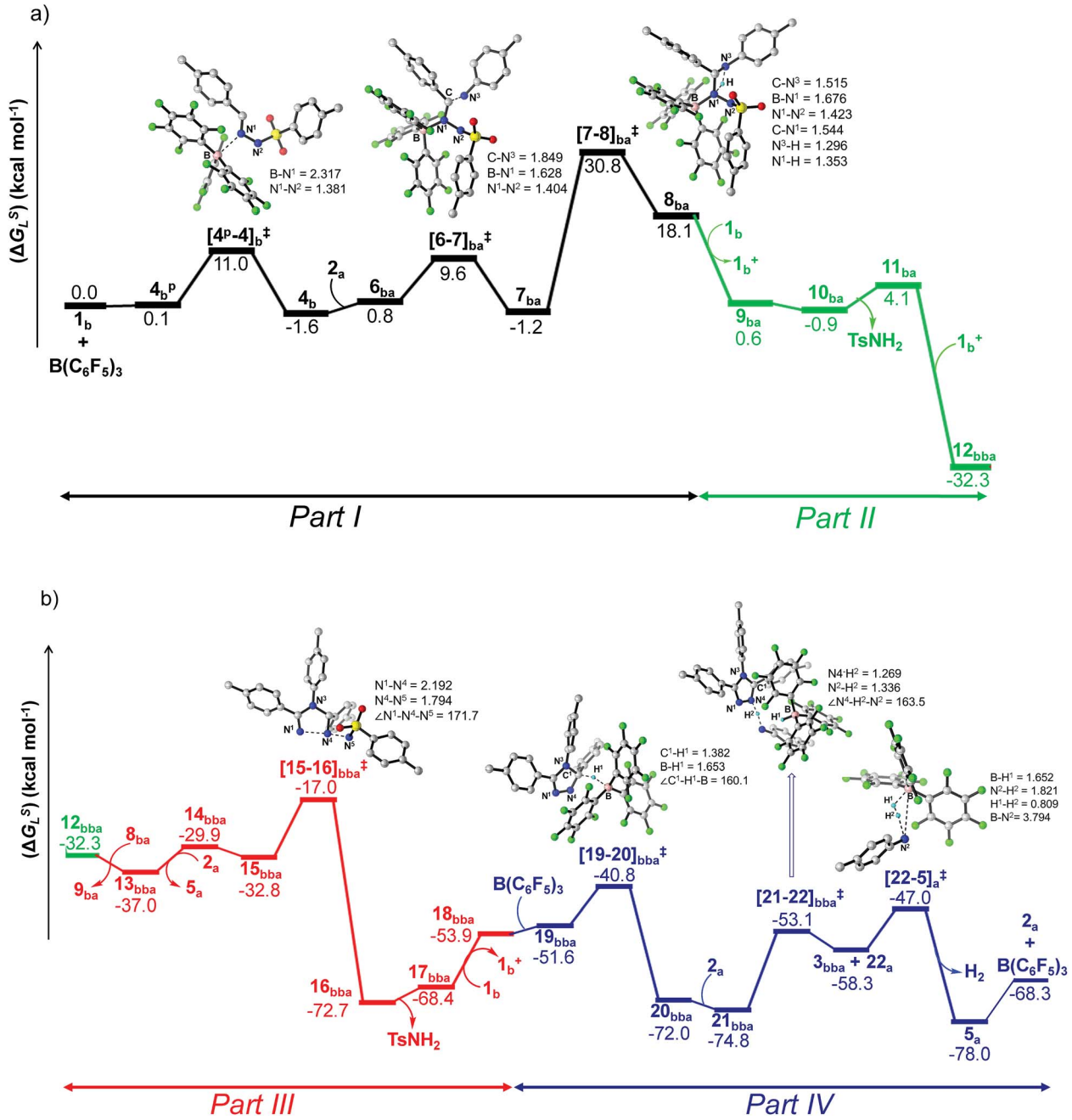

Fig. 1 Energy profile and 3D figures of optimized transition states with selected geometrical parameters for 1,2,4-triazole product ($\mathbf{3_{bba}}$) formation at the B3LYP-D3/TZVP//B3LYP/SVP level. The black, green, red and blue colored pathways represent sections (a) Part I and Part II, and (b) Part III and Part IV, respectively (refer Schemes 6–9). Bond distances are in angstroms (Å) and bond angles are in degrees (°).

dissociation of the N^1–N^2 bond (1.450 Å/2.987 Å = $\mathbf{8_{ba}}$/$\mathbf{9_{ba}}$) and generation of a partial double bond character in the C–N^1 bond (1.568 Å/1.323 Å = $\mathbf{8_{ba}}$/$\mathbf{9_{ba}}$). The N^2 center of the -NHTS unit in $\mathbf{9_{ba}}$ shows significant hydrogen bonding interactions with the H^2 atom connected to the N^3 center, as evidenced by the N^3–H^2 (1.088 Å) and N^2–H^2 (1.622 Å) bond lengths. The dissociation of the $TsNH_2$ fragment is quite evident from $\mathbf{10_{ba}}$ with a shorter N^2–H^2 distance (1.057 Å) and further elongated N^1–N^2 distance (3.634 Å). Complete removal of $TsNH_2$ will generate a highly nucleophilic N^3 center in $\mathbf{11_{ba}}$ which will immediately coordinate with the preformed cationic intermediate $\mathbf{1_b}^+$ to generate substantially stable $\mathbf{12_{bba}}$ (Scheme 7). The coupling of two oppositely charged species is further facilitated by the exothermicity of C–N^3 bond formation.

From $\mathbf{12_{bba}}$ the cyclization step is necessary to generate the triazole product $\mathbf{3_{bba}}$ (Scheme 5). Under these circumstances, it might be conceivable that the liberation of a second $TsNH_2$ unit will facilitate N^1–N^4 bond formation. Thus, protonation at the N^5 center is necessary, similar to the preceding step $\mathbf{8_{ba}}$ → $\mathbf{1_b}^+$ + $\mathbf{9_{ba}}$ in Part II (Scheme 7). Unlike in $\mathbf{8_{ba}}$, the possibility

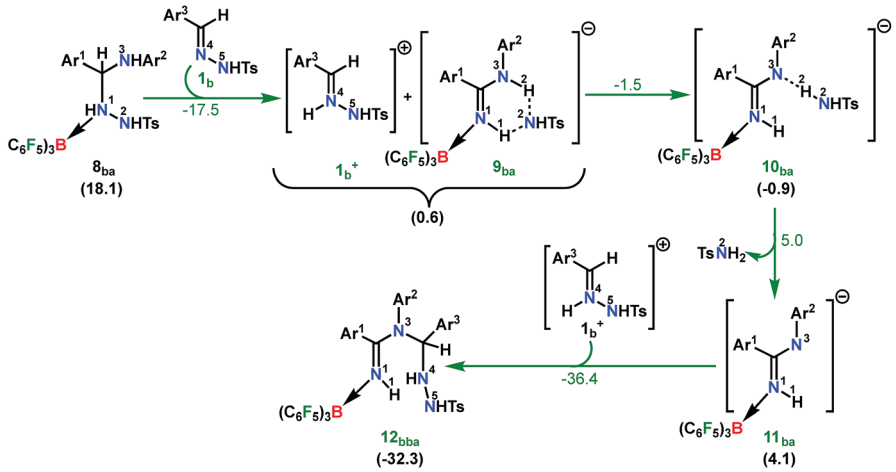

Scheme 7 Part II: the reaction pathway for the formation of the intermediate 12_{bba}. For other information refer the caption of Scheme 6.

of C–H abstraction in $\mathbf{12_{bba}}$ either as a proton or hydride transfer is unfeasible (refer Scheme S18e in the ESI†). However, the formation of cationic species $\mathbf{13_{bba}}$ after protonation along with anionic $\mathbf{9_{ba}}$ generation is possible, but it is less exothermic than the previous transfer ($\mathbf{8_{ba}} \rightarrow \mathbf{1_b}^+ + \mathbf{9_{ba}}$; Schemes 7 and 8). Unfortunately, the addition of protons to any other electronegative center resulted in either high energy intermediates or reaction dead ends (refer Scheme S18f in the ESI†). In order to enhance the nucleophilicity at the N^1 center, $B(C_6F_5)_3$ was uncoordinated in the presence of an aryl amine ($\mathbf{2_a}$) to generate notably unstable $\mathbf{14_{bba}}$ (Scheme 8). Subsequent rearrangement to isomeric $\mathbf{15_{bba}}$ provides adequate structural disposition for facile cyclization to proceed. We have explored numerous possibilities for N^1–N^4 bond formation. However, none of them gave promising alternatives; instead the activation barriers are too high or transition states could not be optimized after numerous attempts (Scheme S18g in the ESI†). The cyclization step involving the transition state $\mathbf{[15\text{-}16]_{bba}}^{\ddagger}$ requires an activation barrier of 15.8 kcal mol^{-1} and it witnesses a progressive removal of the $TsNH_2$ unit.

As expected, the transition vector in $\mathbf{[15\text{-}16]_{bba}}^{\ddagger}$ depicts the breaking of the N^4–N^5 bond (1.794 Å) with the concomitant formation of the N^1–N^4 bond (2.192 Å). Complete removal of $TsNH_2$ affords the saturated triazole intermediate $\mathbf{17_{bba}}$, which is 35.6 kcal mol^{-1} more stable than $\mathbf{15_{bba}}$. Subsequent deprotonation at the N^1 center by $\mathbf{1_b}$ will generate the significantly less stable intermediate $\mathbf{18_{bba}}$.[64] This step is facile with an activation barrier of only 1.6 kcal mol^{-1} (Scheme S19 in the ESI†). The protonated form $\mathbf{1_b}^+$ generated can have two fates: it may either participate in the preceding steps reported in Part II (Scheme 7) or can undergo an endergonic exchange of protons to a free amine ($\mathbf{2_a} + \mathbf{1_b}^+ \rightarrow \mathbf{2_a}^+ + \mathbf{1_b}$; 4.8 kcal mol^{-1}). Generally, the intermediates formed after coupling of the second *N*-tosylhydrazone moiety are highly stable compared to the starting structures and the driving force for the subsequent reactions is the increasing exergonicity towards product formation (refer Fig. 1b). This statement is supported by high-resolution-mass-spectrometry studies which clearly detect a similar skeleton to

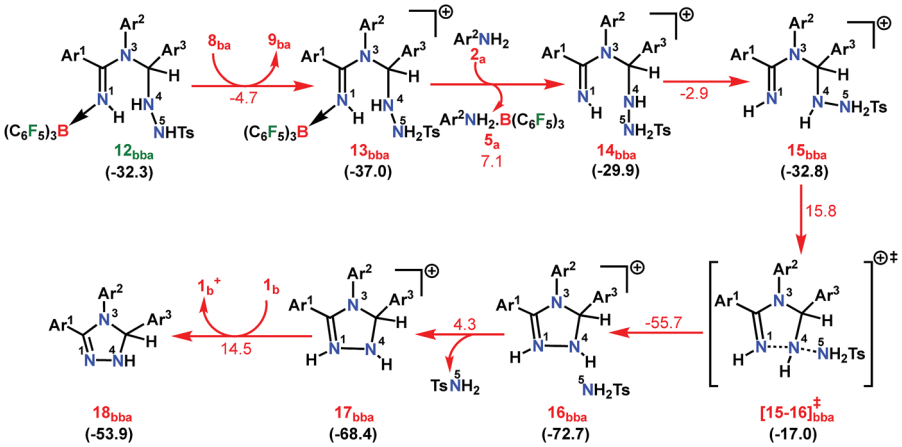

Scheme 8 Part III: the reaction pathway for the formation of the intermediate 18_{bba}. For other information refer the caption of Scheme 6.

$\mathbf{18_{bba}}$ (Fig. S2 in the ESI†). In order to address the positional effect of $B(C_6F_5)_3$ in the cyclization step, we calculated two isomers in which it coordinates to other N centers (N^4 and N^5) in $\mathbf{12_{bba}}$. The resulting intermediates $\mathbf{35_{bba}}$ and $\mathbf{36_{bba}}$ are unstable and did not provide a low energy route to the cyclization step (Scheme S18h in the ESI†). Furthermore, in the absence of $B(C_6F_5)_3$ the cyclization step leading to $\mathbf{18_{bba}}$ encounters a high transition barrier (38.2 kcal mol^{-1}; Scheme S18i in the ESI†) and thus underscores the significance of $B(C_6F_5)_3$ in this current transformation.

In the next step, $\mathbf{18_{bba}}$ undergoes dehydrogenative aromatization[54,55] to furnish triazole $\mathbf{3_{bba}}$ and an ion pair $\mathbf{22_a}$ through $B(C_6F_5)_3$ mediated hydride abstraction ($\mathbf{19_{bba}} \rightarrow \mathbf{20_{bba}}$) followed by proton abstraction involving substituted anilines ($\mathbf{21_{bba}} \rightarrow \mathbf{3_{bba}} + \mathbf{22_a}$; Scheme 9). We have calculated intrinsic activation barriers of 13.1 and 21.7 kcal mol^{-1} for the hydride and proton abstraction steps, respectively. Thereafter, two hydrogen atoms in the ion pair $\mathbf{22_a}$ produce a H_2 molecule *via* the four-membered transition state $\mathbf{[22\text{-}5]_a^{\ddagger}}$ (Scheme 9, Fig. 1b). Liberation of H_2 along with the formation of the frustrated Lewis acid–base pair (FLP) adduct $\mathbf{5_a}$ is facile with a barrier of only 11.3 kcal mol^{-1} (Scheme 9). The evolution of H_2 was also confirmed by the transfer hydrogenation of styrene (*vide supra*, Scheme 4c). Finally, maintaining an endoergic equilibrium, the FLP adduct regenerates $B(C_6F_5)_3$ and substrate $\mathbf{2_a}$.[65] In sum, the computational results do have concurrence with the experimental findings, particularly in understanding the dual role of $B(C_6F_5)_3$ in activating the *N*-tosylhydrazone towards nucleophilic attack and acceptor-less liberation of H_2 with the formation of a FLP (Scheme 9). Additionally, the rate determining step involving intramolecular proton transfer ($\mathbf{7_{ba}} \rightarrow \mathbf{8_{ba}}$; $\Delta^{\ddagger}G_L^{S} = 32.0$ kcal mol^{-1}) can be surmounted at a reaction temperature of 80 °C.[66] Optimized geometries of the transition states with selected geometrical parameters along with the energy profiles are shown in Fig. 1.

For unsymmetrical systems

An equimolar mixture of $\mathbf{1_a}$ and $\mathbf{1_c}$ in the presence of $\mathbf{2_a}$ afforded the unsymmetrical triazole $\mathbf{3_{aca}}$ as the major product (77%) compared to the symmetrical counterpart (*vide supra*; Table 3). To provide reasonable justification for this observation we decided to compare the relative propensity of Lewis acid–base adduct formation of *N*-tosylhydrazones $\mathbf{1_a}$ and $\mathbf{1_c}$ with $B(C_6F_5)_3$ ($B(C_6F_5)_3 \rightarrow \mathbf{4_{a/c}^{P}} \rightarrow \mathbf{4_{a/c}}$). As expected, the formation of $\mathbf{4_a}$ is more facile than $\mathbf{4_c}$ by *ca.* 3.0 kcal mol^{-1} (Fig. S102 in the ESI†). This is in accordance with the experimentally observed equilibrium ratio in Scheme 3b. Eventually the activation barrier for $B(C_6F_5)_3$ coordination is favorable for the –OMe substituent by 3.6 kcal mol^{-1} ($\Delta\Delta^{\ddagger}G_L^{S}$; Fig. S102 in the ESI†). What is more interesting is that the overall energy span for Part I is substantially higher for the –Cl substituent than –OMe (42.5 kcal mol^{-1} *vs.* 33.3 kcal mol^{-1}), clearly indicating the preference for $\mathbf{1_a}$ to undergo $B(C_6F_5)_3$ assisted intra-molecular proton transfer in a facile manner. Therefore, when $\mathbf{8_{aa}}$ couples with another hydrazone unit, the preferred choice will be the chloro-substituted analogue $\mathbf{1_c}$ as most of the $\mathbf{1_a}$ will be available in the adduct form $\mathbf{4_a}$. The combination of $\mathbf{8_{aa}}$ with $\mathbf{1_c}$ will lead directly to $\mathbf{12_{aca}}$ in a favorable fashion with an exothermicity of −50.6 kcal mol^{-1} (Fig. S103 in the ESI†). From $\mathbf{12_{aca}}$, the generation of $\mathbf{16_{aca}}$ requires a barrier of 20.4 kcal mol^{-1} which is almost similar to the value obtained in the previous case (20.0 kcal mol^{-1}: $\mathbf{12_{bba}} \rightarrow \mathbf{16_{bba}}$: Fig. 1b). This barrier is 1.1 kcal mol^{-1} lower than the symmetrical case (Fig. S103 in the ESI†) further supporting the preference for unsymmetrical triazole ($\mathbf{3_{aca}}$) formation (Fig. S103 in the ESI†).

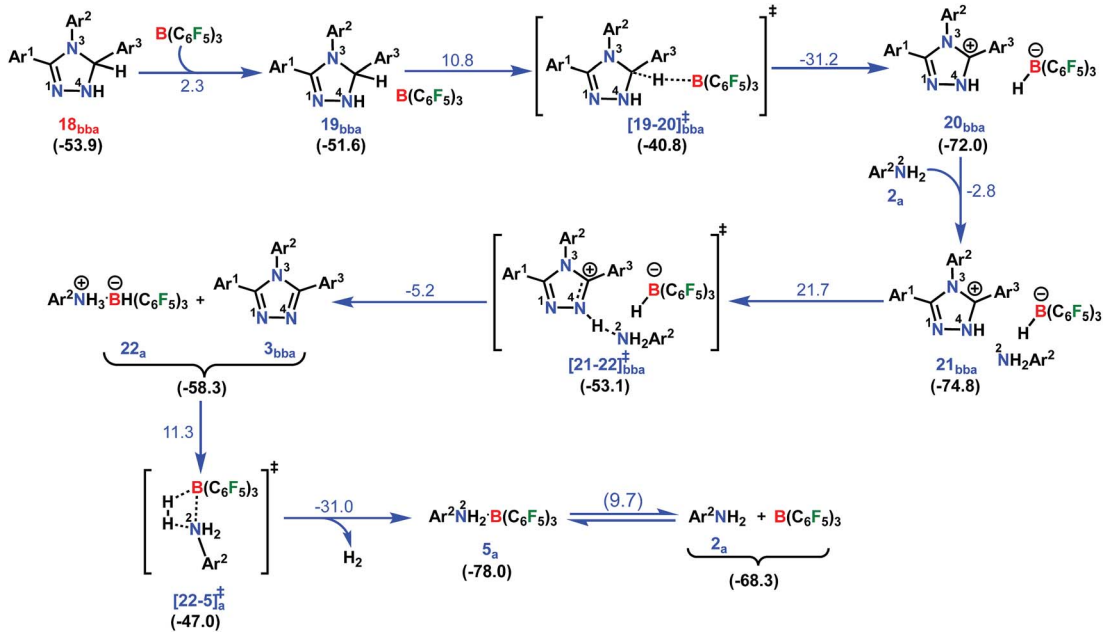

Scheme 9 Part IV: the reaction pathway for the formation of the desired product 1,2,4-triazole complex ($\mathbf{3_{bba}}$) and the hydrogen evolution step. For other information refer the caption of Scheme 6.

After the formation of the triazole ring in $\mathbf{16_{aca}}$, which is 71.5 kcal mol^{-1} more stable than the starting materials, the subsequent $B(C_6F_5)_3$ assisted dehydrogenation follows an analogous mechanism as outlined before (Scheme 9; Fig. 1b).[67]

Conclusions

In summary, we have demonstrated $B(C_6F_5)_3$ catalyzed metal-free, one-pot, dehydrogenative-cyclization of hydrazones with anilines to furnish both symmetrical and unsymmetrical 3,4,5-triaryl-1,2,4-triazoles. The isolation of the *N*-tosylhydrazone-borane adduct is also reported for the first time. Mechanistic experiments and DFT calculations suggest that the $B(C_6F_5)_3$ catalyst serves a dual role: the activation of the hydrazone for the nucleophilic attack and the formation of an FLP for dehydrogenation. Calculations also reveal that the rate-determining step involves intra-molecular hydrogen transfer between the N-centers after aniline gets bonded to the *N*-Tosylhydrazone unit. The chemo-selective, step-economical, oxidant-free and mild reaction protocol could give a potential platform for the increasing focus on main-group catalyzed chemical transformation without using transition metal.

Computational methods

All computations are performed using Gaussian 09 [68] and ADF 2018.103 [69] quantum codes. Geometry optimizations of the saddle points without any symmetry constraints are carried out using the B3LYP hybrid functional[70] in conjunction with the SVP basis set[71] in the Gaussian 09 program package. Harmonic force constants are computed at the optimized geometries to characterize the nature of the stationary points as minima ($N_{img} = 0$) or transition states ($N_{img} = 1$). Transition states are located by using the linear synchronous transit (LST)[72] scan method in which the reaction coordinate was kept fixed at different distances while all other degrees of freedom are relaxed. After the linear transit search, the transition states are optimized by using the default Berny algorithm implemented in the Gaussian 09 code. All transition states are validated by intrinsic reaction coordinate (IRC) calculations. In addition, single point calculations were performed on the B3LYP/SVP optimized structures using the dispersion corrected hybrid functional B3LYP-D3 [73] in conjunction with a large basis set (triple-ζ quality split valence plus polarization, TZVP).[74] The effect of solvation (benzene, dielectric constant $\varepsilon = 2.27$) was assessed by a self-consistent reaction field (SCRF) approach, using the conductor-like polarizable continuum model (CPCM).[75] Tight wave function convergence criteria and an "ultrafine" (99 950) grid were used for the single point calculations. Natural bond orbital (NBO)[76] analysis was performed at the B3LYP-D3/TZVP//B3LYP/SVP level using the NBO Version 3.1 program. QTAIM (quantum theory of atoms in molecules) calculations are also performed to characterize the electron distribution around some selected bonds in the chemical species applying Bader's AIM (atoms-in-molecule) theory.[77] Furthermore, to gain insight into the bonding scenario in the transition state $[\mathbf{4^p\text{-}4}]_b^{\ddagger}$, EDA (energy decomposition analysis) calculations in conjunction with the NOCV (natural orbital for chemical valence)[78] method are undertaken using the ADF 2018.103 package. Implementation and application of the EDA method, which was originally developed by Morokuma[79] and later modified by Ziegler and Rauk,[80] can be found elsewhere.[81–85] The figures provided in the manuscript are generated using ChemDraw Ultra 12.0 and CYLview[86] visualization software.

Conflicts of interest

There are no conflicts to declare.

Acknowledgements

We thank the IISER Kolkata (Start-up grant) for financial support. M. M. G. thanks the SERB (PDF/2017/000028) for the NPDF fellowship. S. De and S. Dutta thank the UGC and CSIR, respectively for senior research fellowships. D. K. acknowledges the funding from the bilateral DST-DFG (INT/FRG/DFG/P-05/2017) scheme and the IISER Kolkata for computational facility. The authors thank Dr. S. Lakhdar (CNRS–ENSI Caen), and Prof. Dr. H. Mayr (LMU Munich) for helpful discussions. Dedicated to Professor Dr. Vinod K. Singh on the occasion of his 60th birthday.

Notes and references

1 W. E. Piers and T. Chivers, *Chem. Soc. Rev.*, 1997, **26**, 345–354.
2 (*a*) K. Ishihara, N. Hananki and H. Yamamoto, *Synlett*, 1993, 577–579; (*b*) K. Ishihara, M. Funahashi, M. Miyata and H. Yamamoto, *Synlett*, 1994, 963–964; (*c*) K. Ishihara, N. Hanaki, M. Funahashi, M. Miyata and H. Yamamoto, *Bull. Chem. Soc. Jpn.*, 1995, **68**, 1721–1730; (*d*) G. Erker, *Dalton Trans.*, 2005, 1883–1890.
3 J. R. Lawson and R. L. Melen, *Inorg. Chem.*, 2017, **56**, 8627–8643.
4 R. L. Melen, L. C. Wilkins, B. M. Kariuki, H. Wadepohl, L. H. Gade, A. S. K. Hashmi, D. W. Stephan and M. M. Hansmann, *Organometallics*, 2015, **34**, 4127–4137.
5 G. Kehr and G. Erker, *Chem. Sci.*, 2016, **7**, 56–65.
6 J. S. McGough, S. M. Butler, I. A. Cade and M. J. Ingleson, *Chem. Sci.*, 2016, **7**, 3384–3389.
7 S. Tamke, Z.-W. Qu, N. A. Sitte, U. Floerke, S. Grimme and J. Paradies, *Angew. Chem., Int. Ed.*, 2016, **55**, 4336–4339.
8 M. Shang, M. Cao, Q. Wang and M. Wasa, *Angew. Chem., Int. Ed.*, 2017, **56**, 13338–13341.
9 C. K. Hazra, J. Jeong, H. Kim, M.-H. Baik, S. Park and S. Chang, *Angew. Chem., Int. Ed.*, 2018, **57**, 2692–2696.
10 M. Shang, J. Z. Chan, M. Cao, Y. Chang, Q. Wang, B. Cook, S. Torker and M. Wasa, *J. Am. Chem. Soc.*, 2018, **140**, 10593–10601.
11 M. Shang, X. Wang, S. M. Koo, J. Youn, J. Z. Chan, W. Yao, B. T. Hastings and M. Wasa, *J. Am. Chem. Soc.*, 2017, **139**, 95–98.
12 Y. Hoshimoto, T. Kinoshita, S. Hazra, M. Ohashi and S. Ogoshi, *J. Am. Chem. Soc.*, 2018, **140**, 7292–7300.

13 D. J. Faizi, A. Issaian, A. J. Davis and S. A. Blum, *J. Am. Chem. Soc.*, 2016, **138**, 2126–2129.
14 H. H. San, S.-J. Wang, M. Jiang and X.-Y. Tang, *Org. Lett.*, 2018, **20**, 4672–4676.
15 C. K. Hazra, N. Gandhamsetty, S. Park and S. Chang, *Nat. Commun.*, 2016, **7**, 13431.
16 P. Smirnov and M. Oestreich, *Organometallics*, 2016, **35**, 2433–2434.
17 Y. Han, S. Zhang, J. He and Y. Zhang, *J. Am. Chem. Soc.*, 2017, **139**, 7399–7407.
18 Y. Ma, L. Zhang, Y. Luo, M. Nishiura and Z. Hou, *J. Am. Chem. Soc.*, 2017, **139**, 12434–12437.
19 K. Chernichenko, A. Madarasz, I. Papai, M. Nieger, M. Leskelae and T. Repo, *Nat. Chem.*, 2013, **5**, 718–723.
20 M.-A. Légaré, M.-A. Courtemanche, É. Rochette and F.-G. Fontaine, *Science*, 2015, **349**, 513–516.
21 D. W. Stephan and G. Erker, *Angew. Chem., Int. Ed.*, 2015, **54**, 6400–6441.
22 W. Meng, X. Feng and H. Du, *Acc. Chem. Res.*, 2018, **51**, 191–201.
23 A. Fukazawa, H. Yamada and S. Yamaguchi, *Angew. Chem., Int. Ed.*, 2008, **47**, 5582–5585.
24 C. M. Moemming, G. Kehr, B. Wibbeling, R. Froehlich, B. Schirmer, S. Grimme and G. Erker, *Angew. Chem., Int. Ed.*, 2010, **49**, 2414–2417.
25 X. Zhao and D. W. Stephan, *Chem. Sci.*, 2012, **3**, 2123–2132.
26 M. M. Hansmann, R. L. Melen, F. Rominger, A. S. K. Hashmi and D. W. Stephan, *Chem. Commun.*, 2014, **50**, 7243–7245.
27 M. M. Hansmann, R. L. Melen, M. Rudolph, F. Rominger, H. Wadepohl, D. W. Stephan and A. S. K. Hashmi, *J. Am. Chem. Soc.*, 2015, **137**, 15469–15477.
28 L. C. Wilkins, J. R. Lawson, P. Wieneke, F. Rominger, A. S. K. Hashmi, M. M. Hansmann and R. L. Melen, *Chem.–Eur. J.*, 2016, **22**, 14618–14624.
29 T. Mahdi and D. W. Stephan, *Chem.–Eur. J.*, 2015, **21**, 11134–11142.
30 V. Fasano, J. E. Radcliffe and M. J. Ingleson, *Organometallics*, 2017, **36**, 1623–1629.
31 Y. Soltani, L. C. Wilkins and R. L. Melen, *Angew. Chem., Int. Ed.*, 2017, **56**, 11995–11999.
32 K. Yuan and S. Wang, *Org. Lett.*, 2017, **19**, 1462–1465.
33 G. M. Brittenham, D. G. Nathan, N. F. Olivieri, M. J. Pippard and D. J. Weatherall, *Lancet*, 2003, **361**, 183–184.
34 R. Tokala, S. Bale, I. P. Janrao, A. Vennela, N. P. Kumar, K. R. Senwar, C. Godugu and N. Shankaraiah, *Bioorg. Med. Chem. Lett.*, 2018, **28**, 1919–1924.
35 Q. Zhang, B. Li, S. Huang, H. Nomura, H. Tanaka and C. Adachi, *Nat. Photonics*, 2014, **8**, 326–332.
36 W. Song, L. Shi, L. Gao, P. Hu, H. Mu, Z. Xia, J. Huang and J. Su, *ACS Appl. Mater. Interfaces*, 2018, **10**, 5714–5722.
37 H. Oka, R. V. Joshi, J. Tanabe, S. Lahiri, D. Vashi and P. Ghogale, *WO Pat.*, WO2006114377A1, 2006.
38 H. Oka, R. V. Joshi, J. Tanabe, S. Lahiri, D. Vashi and P. Ghogale, *US Pat.*, US9113536B2, 2015.
39 B. K. Barman, M. M. Guru, G. K. Panda, B. Maji and R. K. Vijayaraghavan, *Chem. Commun.*, 2019, **55**, 4643–4646.
40 Y. Naito, F. Akahoshi, S. Takeda, T. Okada, M. Kajii, H. Nishimura, M. Sugiura, C. Fukaya and Y. Kagitani, *J. Med. Chem.*, 1996, **39**, 3019–3029.
41 A. Moulin, M. Bibian, A.-L. Blayo, S. El Habnouni, J. Martinez and J.-A. Fehrentz, *Chem. Rev.*, 2010, **110**, 1809–1827.
42 S. Ueda and H. Nagasawa, *J. Am. Chem. Soc.*, 2009, **131**, 15080–15081.
43 S. T. Staben and N. Blaquiere, *Angew. Chem., Int. Ed.*, 2010, **49**, 325–328.
44 H. Wang, Y. Ren, K. Wang, Y. Man, Y. Xiang, N. Li and B. Tang, *Chem. Commun.*, 2017, **53**, 9644–9647.
45 Z. Ye, M. Ding, Y. Wu, Y. Li, W. Hua and F. Zhang, *Green Chem.*, 2018, **20**, 1732–1737.
46 C. Appelt, J. C. Slootweg, K. Lammertsma and W. Uhl, *Angew. Chem., Int. Ed.*, 2013, **52**, 4256–4259.
47 K. L. Bamford, L. E. Longobardi, L. Liu, S. Grimme and D. W. Stephan, *Dalton Trans.*, 2017, **46**, 5308–5319.
48 T. C. Johnstone, G. N. J. H. Wee and D. W. Stephan, *Angew. Chem., Int. Ed.*, 2018, **57**, 5881–5884.
49 C. Tang, Q. Liang, A. R. Jupp, T. C. Johnstone, R. C. Neu, D. Song, S. Grimme and D. W. Stephan, *Angew. Chem., Int. Ed.*, 2017, **56**, 16588–16592.
50 R. L. Melen, *Angew. Chem., Int. Ed.*, 2018, **57**, 880–882.
51 C. Gunanathan and D. Milstein, *Science*, 2013, **341**, 249.
52 R. H. Crabtree, *Chem. Rev.*, 2017, **117**, 9228–9246.
53 Z. Lu, L. Schweighauser, H. Hausmann and H. A. Wegner, *Angew. Chem., Int. Ed.*, 2015, **54**, 15556–15559.
54 M. Kojima and M. Kanai, *Angew. Chem., Int. Ed.*, 2016, **55**, 12224–12227.
55 (*a*) A. F. G. Maier, S. Tussing, T. Schneider, U. Floerke, Z.-W. Qu, S. Grimme and J. Paradies, *Angew. Chem., Int. Ed.*, 2016, **55**, 12219–12223; (*b*) Z.-J. Cai, X.-M. Lu, Y. Zi, C. Yang, L.-J. Shen, J. Li, S.-Y. Wang and S.-J. Ji, *Org. Lett.*, 2014, **16**, 5108–5111; (*c*) Z. Chen, Q. Yan, Z. Liu and Y. Zhang, *Chem.–Eur. J.*, 2014, **20**, 17635–17639; (*d*) J.-P. Wan, D. Hu, Y. Liu and S. Sheng, *ChemCatChem*, 2015, **7**, 901–903; (*e*) J.-P. Wan, S. Cao and Y. Liu, *Org. Lett.*, 2016, **18**, 6034–6037; (*f*) S. Panda, P. Maity and D. Manna, *Org. Lett.*, 2017, **19**, 1534–1537.
56 Z. Mo, A. Rit, J. Campos, E. L. Kolychev and S. Aldridge, *J. Am. Chem. Soc.*, 2016, **138**, 3306–3309.
57 M. K. Barman, S. Waiba and B. Maji, *Angew. Chem., Int. Ed.*, 2018, **57**, 9126–9130.
58 CCDC 1866759 contains the supplementary crystallographic data for this paper.
59 S. Keess and M. Oestreich, *Chem. Sci.*, 2017, **8**, 4688–4695.
60 Q. Wang, J. Chen, X. Feng and H. Du, *Org. Biomol. Chem.*, 2018, **16**, 1448–1451.
61 T. Mondal, S. Dutta, S. De, D. Thirumalai and D. Koley, *J. Phys. Chem. A*, 2019, **123**, 565–581.
62 S. Dutta, B. Maity, D. Thirumalai and D. Koley, *Inorg. Chem.*, 2018, **57**, 3993–4008.
63 (*a*) D. Roy and R. B. Sunoj, *Org. Lett.*, 2007, **9**, 4873–4876; (*b*) K. Ando, *J. Org. Chem.*, 2010, **75**, 8516–8521; (*c*) R. Sharma, M. Thorley, J. P. McNamara, C. I. F. Watt and N. A. Burton, *Phys. Chem. Chem. Phys.*, 2008, **10**, 2475–2487.

64 Deprotonation from the N^4 center will afford highly unstable intermediates ($\Delta G_L^S = 37.6$ kcal mol^{-1}) compared to **17bba**.
65 L. Greb, S. Tamke and J. Paradies, *Chem. Commun.*, 2014, **50**, 2318–2320.
66 Y. Ma, S.-J. Lou, G. Luo, G. Zhan, M. Nishiura, Y. Luo and Z. Hou, *Angew. Chem., Int. Ed.*, 2018, **57**, 15222–15226.
67 The energy span in Part IV ($\mathbf{18_{aca}} \rightarrow \mathbf{20_{aca}}$) is reduced by *ca.* 4.0 kcal mol^{-1} when intermediates for the step $\mathbf{17_{aca}} \rightarrow \mathbf{18_{aca}}$ were optimized in benzene continuum (B3LYP/SVP(CPCM) level).
68 M. J. Frisch, G. W. Trucks, H. B. Schlegel, G. E. Scuseria, M. A. Robb, J. R. Cheeseman, G. Scalmani, V. Barone, B. Mennucci, G. A. Petersson, H. Nakatsuji, M. Caricato, X. Li, H. P. Hratchian, A. F. Izmaylov, J. Bloino, G. Zheng, J. L. Sonnenberg, M. Hada, M. Ehara, K. Toyota, R. Fukuda, J. Hasegawa, M. Ishida, T. Nakajima, Y. Honda, O. Kitao, H. Nakai, T. Vreven, J. A. Montgomery Jr, J. E. Peralta, F. Ogliaro, M. Bearpark, J. J. Heyd, E. Brothers, K. N. Kudin, V. N. Staroverov, T. Keith, R. Kobayashi, J. Normand, K. Raghavachari, A. Rendell, J. C. Burant, S. S. Iyengar, J. Tomasi, M. Cossi, N. Rega, J. M. Millam, M. Klene, J. E. Knox, J. B. Cross, V. Bakken, C. Adamo, J. Jaramillo, R. Gomperts, R. E. Stratmann, O. Yazyev, A. J. Austin, R. Cammi, C. Pomelli, J. W. Ochterski, R. L. Martin, K. Morokuma, V. G. Zakrzewski, G. A. Voth, P. Salvador, J. J. Dannenberg, S. Dapprich, A. D. Daniels, O. Farkas, J. B. Foresman, J. V. Ortiz, J. Cioslowski and D. J. Fox, *Gaussian 09, Revision D.01*, Gaussian, Inc., Wallingford CT, 2013.
69 (*a*) G. te Velde, F. M. Bickelhaupt, E. J. Baerends, C. Fonseca Guerra, S. J. A. van Gisbergen, J. G. Snijders and T. Ziegler, *J. Comput. Chem.*, 2001, **22**, 931–967; (*b*) *GUI 2013*, SCM, Amsterdam, The Netherlands, https://www.scm.com.
70 (*a*) A. D. Becke, *J. Chem. Phys.*, 1993, **98**, 5648–5652; (*b*) C. Lee, W. Yang and R. G. Parr, *Phys. Rev. B: Condens. Matter Mater. Phys.*, 1988, **37**, 785–789.
71 A. Schäfer, H. Horn and R. J. Ahlrichs, *J. Chem. Phys.*, 1992, **97**, 2571–2577.
72 T. A. Helgren and W. N. Lipscomb, *Chem. Phys. Lett.*, 1977, **49**, 225–232.
73 S. Grimme, J. Antony, S. Ehrlich and H. A. Krieg, *J. Chem. Phys.*, 2010, **132**, 154104–154122.
74 A. Schafer, C. Huber and R. Ahlrichs, *J. Chem. Phys.*, 1994, **100**, 5829–5835.
75 M. Cossi, G. Scalmani, N. Rega and V. Barone, *J. Comput. Chem.*, 2003, **24**, 669–681.
76 (*a*) E. D. Glendening, A. E. Reed, J. E. Carpenter and F. Weinhold, *NBO Version 3.1*, University of Wisconsin, Madison, WI, 2001; (*b*) A. E. Reed, L. A. Curtiss and F. Weinhold, *Chem. Rev.*, 1988, **88**, 899–926.
77 R. F. W. Bader, *Chem. Rev.*, 1991, **91**, 893–928.
78 (*a*) M. Mitoraj and A. Michalak, *Organometallics*, 2007, **26**, 6576–6580; (*b*) M. P. Mitoraj, A. Michalak and T. Ziegler, *J. Chem. Theory Comput.*, 2009, **5**, 962–975.
79 (*a*) K. Morokuma, *J. Chem. Phys.*, 1971, **55**, 1236–1244; (*b*) K. Kitaura and K. Morokuma, *Int. J. Quantum Chem.*, 1976, **10**, 325–340.
80 (*a*) T. Ziegler and A. Rauk, *Inorg. Chem.*, 1979, **18**, 1755–1759; (*b*) T. Ziegler and A. Rauk, *Theor. Chim. Acta*, 1977, **46**, 1–10.
81 T. Mondal, S. Dutta, S. De and D. Koley, *J. Org. Chem.*, 2019, **84**, 257–272.
82 S. Dutta, T. Mondal, S. De, K. Rudra and D. Koley, *Inorg. Chim. Acta*, 2019, **485**, 162–172.
83 G. Frenking, K. Wichmann, N. Fröhlich, C. Loschen, M. Lein, J. Frunzke and V. M. Rayon, *Coord. Chem. Rev.*, 2003, **238–239**, 55–82.
84 F. M. Bickelhaupt and K. N. Houk, *Angew. Chem., Int. Ed.*, 2017, **56**, 10070–10086.
85 T. Mondal, S. De and D. Koley, *Inorg. Chem.*, 2017, **56**, 10633–10643.
86 C. Y. Legault, *CYLview, 1.0b*, Université de Sherbrooke, 2009, see http://www.cylview.org.